Ultrasound in Med. & Biol., Vol. 45, No. 5, pp. 1151–1163, 2019

0301-5629/$ - see front matter

https://doi.org/10.1016/j.ultrasmedbio.2018.12.014

● *Original Contribution*

SONOTHROMBOLYSIS WITH MAGNETICALLY TARGETED MICROBUBBLES

Marie de Saint Victor, Lester C. Barnsley,[1] Dario Carugo,[2] Joshua Owen, Constantin C. Coussios, and Eleanor Stride

Institute of Biomedical Engineering, Department of Engineering Science, University of Oxford, Oxford, United Kingdom

(*Received* 23 *May* 2018; *revised* 18 *December* 2018; *in final from* 22 *December* 2018)

Abstract—Microbubble-enhanced sonothrombolysis is a promising approach to increasing the tolerability and efficacy of current pharmacological treatments for ischemic stroke. Maintaining therapeutic concentrations of microbubbles and drugs at the clot site, however, poses a challenge. The objective of this study was to investigate the effect of magnetic microbubble targeting upon clot lysis rates *in vitro*. Retracted whole porcine blood clots were placed in a flow phantom of a partially occluded middle cerebral artery. The clots were treated with a combination of tissue plasminogen activator (0.75 μg/mL), magnetic microbubbles (~10^7 microbubbles/mL) and ultrasound (0.5 MHz, 630-kPa peak rarefactional pressure, 0.2-Hz pulse repetition frequency, 2% duty cycle). Magnetic targeting was achieved using a single permanent magnet (0.08–0.38 T and 12-140 T/m in the region of the clot). The change in clot diameter was measured optically over the course of the experiment. Magnetic targeting produced a threefold average increase in lysis rates, and linear correlation was observed between lysis rate and total energy of acoustic emissions. (E-mail: eleanor.stride@eng.ox.ac.uk)

Key Words: **Magnetic targeting, Microbubbles, Thrombolysis, Ultrasound, Clot, Passive cavitation detection, Drug delivery.**

INTRODUCTION

Despite recent therapeutic advances, ischemic stroke remains a leading cause of disability and mortality worldwide (Feigin et al. 2017; GBD 2013 Mortality and Causes of Death Collaborators 2015). At present, intravenous tissue plasminogen activator (tPA) is the only thrombolytic drug recommended by the British National Institute of Health and Care Excellence (NICE 2008) and the U.S. Food and Drug Administration (FDA 1996). It carries, however, the risk of potentially fatal side effects including intracranial haemorrhage. As a result, intravenous tPA administration is subject to rigid exclusion criteria (American College of Emergency Physicians and American Academy of Neurology 2013; Feigin 2017). Among the most limiting of these is the therapeutic time frame for intravenous administration of the drug (Barber et al. 2001). In a study conducted with the California Acute Stroke Pilot Registry, only 4.3% of all ischaemic stroke patients arrived in the emergency department within the recommended 3-h window after stroke onset and were thus eligible for tPA. Of equal concern is the fact that even if all patients had arrived within the required time frame, only 28.6% of them would have been eligible for thrombolytic treatment (California Acute Stroke Pilot Registry Investigators 2005).

Against this background, there is a clear need for an adjuvant therapy that improves the tolerability and efficacy of thrombolytic treatment. Sonothrombolysis, that is, the use of ultrasound (US) for enhanced thrombolysis, is a minimally or non-invasive physical approach that can be used to enhance the action of tPA, thereby reducing the required dose or facilitating clot breakdown in the absence of a drug. Multiple *in vitro* and *in vivo* studies have indicated that intravenously administered microbubbles can significantly improve the rate of clot breakdown, with or without concomitant

Address correspondence to: Eleanor Stride, Institute of Biomedical Engineering, University of Oxford, Old Road Campus Research Building, Oxford OX3 7DQ, UK. E-mail: eleanor.stride@eng.ox.ac.uk

[1] Present address: Jülich Centre for Neutron Science (JCNS) at Heinz Maier-Leibnitz Zentrum (MLZ), Forschungszentrum Jülich GmbH, Lichtenbergstrasse 1, D-85748 Garching, Germany.

[2] Present address: Faculty of Engineering and Physical Sciences, Institute for Life Sciences (IfLS), University of Southampton, Highfield, Southampton SO17 1BJ, UK.

use of a thrombolytic drug (Lu et al. 2016; Schleicher et al. 2016). Several clinical trials have also reported accelerated recanalisation of occluded vessels (Molina et al. 2006; Perren et al. 2008). The echogenicity of microbubbles may further improve patient tolerability by enabling continuous treatment monitoring (Xie et al. 2009a).

Further work is, however, necessary to improve the tolerability and efficacy of sonothrombolysis protocols. In particular, the hydrodynamic conditions in occluded vessels represent a major challenge because they severely limit the number of microbubbles that can be delivered to and retained at the site of a thrombus (de Saint Victor et al. 2017). Conjugation of antibodies to the microbubble surface has been investigated as a means of increasing the proximity between microbubbles and the thrombus surface, thereby enhancing their lytic effect (Hagisawa et al. 2013; Hua et al. 2014). This approach, however, does not address the challenge of delivering a sufficient concentration of microbubbles to the clot initially. The objective of the present study was therefore to investigate whether magnetic targeting could be used to improve both the delivery and the retention of microbubbles to an *in vitro* clot model and whether this could enhance enzymatic sonothrombolysis. In addition, the feasibility of non-invasive acoustic methods for treatment monitoring was evaluated.

METHODS

Clot model

Fresh plasma, employed as the flow medium, was prepared by collecting whole blood from the aortic artery of a female Large White × Landrace breed pig into citrated blood bags (CPDA-1, Fenwal Inc., Lake Zurich, IL, USA) and spinning the sample at 4400 rpm in a 15-cm-radius centrifuge for 20 min at room temperature to separate blood components. The plasma was stored at −80°C until use. It was defrosted at 37°C for at least 15 min before the experiments. All animal work was approved by an animal care and ethics review committee and conformed to the UK Animals (Scientific Procedures) Act 1986.

Clots were formed around silk sutures according to a protocol similar to that described by Meunier et al. (2007). Briefly, 4-O braided silk sutures (Ethicon US LLC, Somerville, NJ, USA) were threaded through 3.4-mm-inner-diameter, 60-mm-long borosilicate cylinders (Aimer Products, Enfield, UK). Each cylinder was placed in an additive-free 13-mm-inner-diameter Vacutainer tube (BD, Franklin Lakes, NJ, USA). Two-milliliter blood samples were then aliquoted into the Vacutainers and incubated for 6 h in a water bath at 37°C, then at 4°C for 24 h to allow retraction. The clots were typically of cylindrical shape, with a diameter of 1.7 ± 0.5 mm and a length of approximately 30 mm. These were stored for at least 48 h before use, and kept for up to 15 d in degassed phosphate-buffered saline (PBS) at 4°C. Holland et al. (2008) found, in a similar clot model, that clot age has no effect on response to tPA within this time frame.

Flow loop

The experiments were carried out in a 50 × 80 × 55-cm Lucite tank containing approximately 120 L of filtered, de-ionised and degassed water, which was maintained at 37 ± 1.5°C with a heating circulator (GD100, Grant Instruments, Cambridge, UK). The clots were placed in a flow chamber consisting of an optically and acoustically transparent polyolefin tube (3.2-mm inner diameter and 0.18-mm wall thickness, Heatshrink-Online Ltd, Huntingdon, UK). The internal diameter of the tube was selected to correspond to the typical dimensions of the middle cerebral artery (Serrador et al. 2000), one of the cerebral vessels most commonly affected by ischaemic stroke (Demchuk et al. 2001). A solution of dilute plasma (1.25% v/v fresh-frozen plasma in PBS) was circulated once through the chamber at the rate of 3 mL/min by a peristaltic pump (Minipuls 2, Gilson Inc., Middleton, WI, USA). The flow rate was selected to obtain a mean blood velocity past the clot at the lower end of the range observed in a partially occluded middle cerebral artery (Ogata et al. 2004). Lipid-shelled magnetic microbubbles were infused continuously, along with tPA, into the diluted plasma at the rate of 140 μL/min using a syringe pump (World Precision Instruments Ltd, Hitchin, UK). The final concentrations of tPA and microbubbles in the diluted plasma were 0.75 μg/mL and $8.1 \times 10^6 \pm 1.2 \times 10^5$ microbubbles/mL, respectively. Four experimental groups were defined: exposure to tPA only, US + tPA, US + tPA + microbubbles (no external magnet) and US + tPA + microbubbles + external magnet.

Magnetic microbubble preparation

Phosphate-buffered saline was sourced from Sigma Aldrich Corporation (St Louis, MO, USA). Tissue plasminogen activator (Actilyse, Boehringer Ingelheim Pharma GmbH & Co. KG, Ingelheim am Rhein, Germany) was reconstituted in water to the concentration of 1 mg/mL and stored in 400-μL aliquots at −80°C. Under these storage conditions, the enzyme is stable for up to a year (Alkatheri 2013; Jaffe et al. 1989). The phospholipid 1, 2-distearoyl-*sn*-glycero-3-phosphocholine (DSPC) was purchased from Avanti Polar Lipids Inc. (Alabaster, AL, USA). The ferrofluid (10-nm spherical magnetite

nanoparticles in isoparaffin, 10% volume fraction) was obtained from Liquids Research Ltd (Bangor, UK).

The protocol for magnetic microbubble preparation was based on the method first described by Stride et al. (2009). The microbubbles were prepared by sonication using a 22.5-kHz ultrasonic cell disruptor (Microson XL, Misonix Inc., Farmingdale, NY, USA) operating at level 4, corresponding to an output power of 8 WRMS. Briefly, 15 mL of de-ionised water was added to 15 mg of DSPC. The sonicating probe was first inserted into this solution for 90 s to disperse the lipid; then it was placed at the air−liquid interface for 15 s to entrain air. Subsequently, 15 μL of the ferrofluid was added to the solution. The microbubble solution was then sonicated again for 30 s with the probe tip fully inserted into the fluid and for 15 s with the probe tip at the air−liquid interface. The vial was manually shaken vigorously for 45 s. Microbubble concentration and size were assessed as previously described by Sennoga et al. (2010). A 10-μL sample was placed on a microscope slide, and 25 images were taken with a × 40 objective. The images were then analysed using purpose-written software in MATLAB (The MathWorks Inc., Natick, MA, USA) to count particles of diameters ranging from 0.2 μm (~2 pixels) to 15 μm.

Magnetic targeting

The magnetic field was applied as illustrated in Figure 1, using a single 12.7-mm cubic permanent magnet element (N52 grade NdFeB, NeoTexx, Berlin, Germany). It was placed below the clot at an angle of 45°, its upper vertex in contact with the flow channel directly below the US focus. During experiments that did not involve magnetic targeting, the magnet was replaced by a stainless-steel block of identical dimensions to maintain a comparable sound field.

The magnetic field and the magnetic field gradient in the flow chamber were first computed using a numerical model developed by Barnsley et al. (2015). The magnetisation value of the magnet, an essential input parameter to the model, was determined experimentally by measuring the field profile of a single NdFeB element using a three-axis Hall probe connected to a Model 460 three-channel gaussmeter (Lake Shore Cryotronics Inc., Westerville, OH, USA). The field profile was fitted to an analytical expression for the field generated by a cuboid (Engel-Herbert and Hesjedal 2005), yielding a magnetisation value of 1.087×10^6 A/m.

Before the sonothrombolysis experiment, magnetic targeting efficiency was evaluated. In these experiments, the clot was replaced by a light-coloured phantom of the same dimensions so as to facilitate visualisation of the dark brown microbubble solution. A 1-mL bolus was injected into the flow, and images were acquired at 30 frames/s with a digital camera (Canon EOS 500D, Canon Ltd., Reigate, UK). The images were processed with purpose-written code in MATLAB to quantify

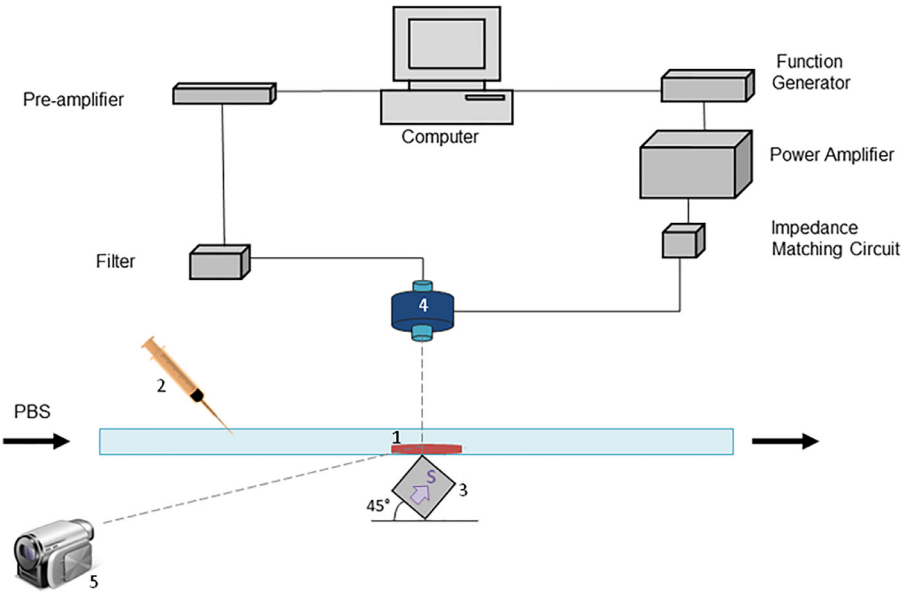

Fig. 1. Overview of the experimental setup. The clot (1) was placed in an acoustically and optically transparent chamber through which a dilute plasma solution (1.25% v/v in PBS) was flowing. Tissue plasminogen activator and microbubbles were continuously injected into the flow with an infusion pump (2). A magnet (3) enabled magnetic retention of the microbubbles at the clot site. Ultrasound exposure and acoustic monitoring were performed by a pair of coaxial transducers (0.5 and 7.5 MHz, respectively) (4). Lysis progress was monitored using a digital camera (5). PBS = phosphate-buffered saline.

retention of magnetic material over 12 s. In each frame, the region of interest (ROI) was defined as a 3-mm-wide window around the axis of the US transducer. NR(t), the "normalised retention" at a given time point t, was defined as

$$\mathrm{NR}(t) = \frac{I(t)-I(t_0)}{I(t_1)-I(t_0)} \quad (1)$$

where $I(t)$ is the total gray-scale intensity in the ROI at time t, t_0 is baseline time (before bolus injection), and t_1 corresponds to bolus arrival in the ROI.

Ultrasound exposure and monitoring

For the US experiments, two US transducers were mounted coaxially, as described by Hockham et al. (2010). The US source was a focused, circular, single-element, 0.5-MHz transducer (Sonic Concepts, Bothell, WA, USA). The transducer centre frequency was chosen to balance considerations of treatment tolerability and efficacy. Lower-frequency US is more effective at breaking down blood clots (Nedelmann et al. 2005; Schafer et al. 2005) and is less attenuated by tissue and bone, but tolerability concerns have been raised in several studies conducted with low- to mid-frequency transcranial US (60−300 kHz) (Daffertshofer et al. 2005; Nedelmann et al. 2008). This transducer had a diameter of 64 mm and a focal length of 62.64 mm. The measured −3-dB focal volume dimensions were 4 mm laterally and 37 mm axially. It was driven by a function generator (3325DA, Agilent Technologies Inc., Santa Clara, CA, USA) and connected to a power amplifier (A300, Electronics & Innovation Ltd., Rochester, NY, USA) with a custom-made impedance matching network (Sonic Concepts). The clot was exposed for 60 min to 5×10^4 cycle bursts at a 0.2-Hz pulse repetition frequency, corresponding to a 2% duty cycle. The peak rarefactional pressure at the focus was set to 630 kPa, measured in the absence of the clot and vessel with a calibrated fibre-optic hydrophone (Precision Acoustics, Dorchester, UK).

Passive cavitation detection (PCD) of acoustic emissions was carried out using a focused, circular, single-element, 7.5-MHz transducer (Panametrics V320-SU, Olympus Inc., Waltham, MA, USA). This PCD transducer had a focal length of 75 mm, an aperture of 12.5 mm and −3-dB focal volume dimensions of 1.2 mm laterally and 37.6 mm axially. Before each experiment, the foci of the 0.5-MHz and the PCD transducers were aligned with the surface of the clot using the PCD transducer in pulse-echo mode. The PCD signal was acquired using a 2-MHz high-pass filter (Allen Avionics, Mineola, NY, USA) to block signals at the fundamental frequency. The filter was connected to a pre-amplifier to achieve × 25 signal amplification (SR445A, Stanford Research Systems, Sunnyvale, CA, USA). The first 2 ms of each 100-ms pulse was then acquired into a binary file at 10^8 samples/s using a data acquisition card and control software written in LabView (National Instruments, Austin, TX, USA). As the microbubbles were constantly replenished in the flow chamber, cavitation was expected to be consistent throughout treatment. Signal acquisition was therefore triggered for every 10th burst to reduce data volume.

Image acquisition

Lysis progress was assessed from the changes in clot diameter throughout treatment. Images of the clot were captured every 30 s using a digital camera. Clot outlines were detected offline using custom-written code in MATLAB, and the maximum depth of clot lysis (*i.e.*, maximum change in diameter compared with baseline) was computed at each time point in a 3-mm-wide window around the axis of the US transducer. Linear regression on the depth of lysis over the 60 min of treatment yielded the overall lytic rate. In the group with magnetic targeting, magnetic material gradually accumulated near the clot until it obstructed the view in the ROI, so the regression was limited to the period before full obstruction (at least the first 20 images).

PCD signal processing

The acoustic emissions recorded during treatment were processed as follows. The first 90 μs of the burst were discarded to account for the acoustic time of flight from the 0.5-MHz transducer to the focal region and back to the PCD transducer. The signal was zero padded and windowed using a Hann window, and its power spectral density was derived by fast Fourier transform. The total power emitted in the frequency range 2−5 MHz was computed by integrating the power spectral density over the corresponding frequency range. The acoustic emissions thus computed for each burst were summed over the whole duration of treatment, yielding the total energy of acoustic emission for that treatment.

Histologic analysis

After treatment completion, the clots were immersed in formalin and fixed in paraffin. Slides of 5 μm thickness were prepared, stained with eosin and haematoxylin and analysed in bright-field microscopy (Ti Eclipse, Nikon Instruments Inc., Melville, NY, USA) using a × 20 objective (S Plan Fluor EWLD, Nikon).

Clot debris analysis

Secondary embolism caused by circulation of clot debris is a potential risk of sonothrombolysis. To assess clot debris size, 15 mL of effluent was collected halfway through treatment and immediately stored at −20°C.

The samples were then defrosted for 12 h at 4°C. This low temperature was maintained so as to inhibit the enzymatic activity of tPA, limiting further breakdown of the clot debris. One hundred-microliter samples of the solution were analysed with an optical particle sizer (Accusizer 780, Particle Sizing Systems, Santa Barbara, CA, USA), designed to size particles between 0.5 and 400 μm. Three samples were analysed for each clot.

Statistics

Differences among experimental groups were analysed in MATLAB using a two-way analysis of variance with *post hoc* Tukey honestly-significant-difference testing for multiple comparisons between groups. Statistical significance was defined as $p < 0.05$ (denoted by an asterisk in the figures). Data with greater significance ($p < 0.01$) are denoted by two asterisks.

RESULTS

Magnetic field characterisation

A numerical simulation was performed to map the magnetic field and the magnetic field gradient in the phantom vessel. As expected, the magnitudes of both were symmetric about the 0xz plane (data not shown), but not about the 0yz plane (Fig. 2), because of the orientation of the magnetisation vector. The magnet produced a strong field and field gradient within the vessel. Both decreased rapidly with increasing distance from the upper vertex of the magnet.

It should be noted that the numerical model breaks down in the region approximately 1 mm from the magnet. This is due to the approximation of the magnetic medium as a lattice of evenly distributed point dipoles, which is no longer valid in the short range. Precise estimation of the magnetic field in this narrow region is, however, not relevant to the present study, as the region is occupied by the clot and no microbubbles can be present. Magnetic targeting takes place in the liquid above the clot, where valid predictions can be made, and in a range of positions inside the channel 1.5 to 10 mm from the magnet, predicted values for the magnetic field are within 0.38−0.08 T; the magnetic field gradient varies from 140 to 12 T/m.

Magnetic microbubble retention

Figure 3 shows a photograph of the experimental flow model after injection of a bolus of microbubble stock solution into the flow, past a clot phantom. In the absence of a magnet and of US exposure (Fig. 3a), the microbubbles float to the top of the flow chamber because of their buoyancy and do not come into contact with the clot phantom. In the presence of a magnet (Fig. 3b), the magnetic material accumulates in a narrow region (~3 mm wide) that coincides with the focus of the 0.5-MHz transducer. As the clot is narrower than the tube, Figure 3c illustrates that some magnetic material collects at the bottom of the flow chamber on either side of the clot, where its contribution to lysis will be limited. A substantial proportion of the magnetic material, however, accumulates at the target site, directly on top of the clot.

The proportion of microbubbles retained in the model is quantified in Figure 4. In the absence of a magnet, the total gray-scale intensity remained constant in the focal region over the period of observation, indicating no change in the amount of magnetic material. On the other hand, total gray-scale intensity increased rapidly in the presence of a magnetic field, confirming a large increase in local concentration.

Effect of magnetic targeting on lysis rates

Six clots were treated in each experimental group. Maximum depth of clot lysis was measured every 30 s over the 60 min of treatment. Linear regression was carried out on the maximum depth of lysis and yielded an acceptable fit on average over all experimental groups ($R^2 = 0.75 \pm 0.3$). In the two experimental groups involving microbubbles, the linear fit was very good ($R^2 = 0.95 \pm 0.04$).

Figure 5 illustrates the rates of lysis in all four experimental groups. Negligible lysis was observed in the clots treated with tPA only or with tPA + US ($1.3 \pm 1.4 \times 10^{-3}$ mm/min and $2.9 \pm 2.8 \times 10^{-3}$ mm/min, respectively). Lysis rates were substantially increased in the presence of microbubbles ($11.2 \pm 4.1 \times 10^{-3}$ mm/min with US + tPA + microbubbles, non-significant); these rates were further accelerated (× 3.3 on average) with a magnetic field ($36.6 \pm 23.4 \times 10^{-3}$ mm/min with US + tPA + microbubbles + magnet, $p < 0.05$).

The effect of treatment on clot structure was investigated on H&E-stained clot samples (Fig. 6). The surface of clots treated without microbubbles (Fig. 6a, b) was smooth. On the clot treated with tPA with US, it was not possible to identify with precision the focal region. In the samples treated with US + tPA + microbubbles, the damaged region has a smooth surface and several small areas of erythrocyte depletion (Fig. 6c, direction of US exposure indicated by the *black arrow*). Closer inspection reveals that these cavities still contain fibrin. These observations are in agreement with the report by Petit et al. (2012). All of the samples treated with US + tPA + microbubbles + magnet were entirely lysed at the transducer focus after 60 min of treatment. Figure 6d illustrates the remaining clot fragments on either side of the lysed region. Numerous erythrocyte-depleted cavities with accumulation of magnetic material are present throughout the clot. Please note that in this case the clot was severed in two by the treatment. In

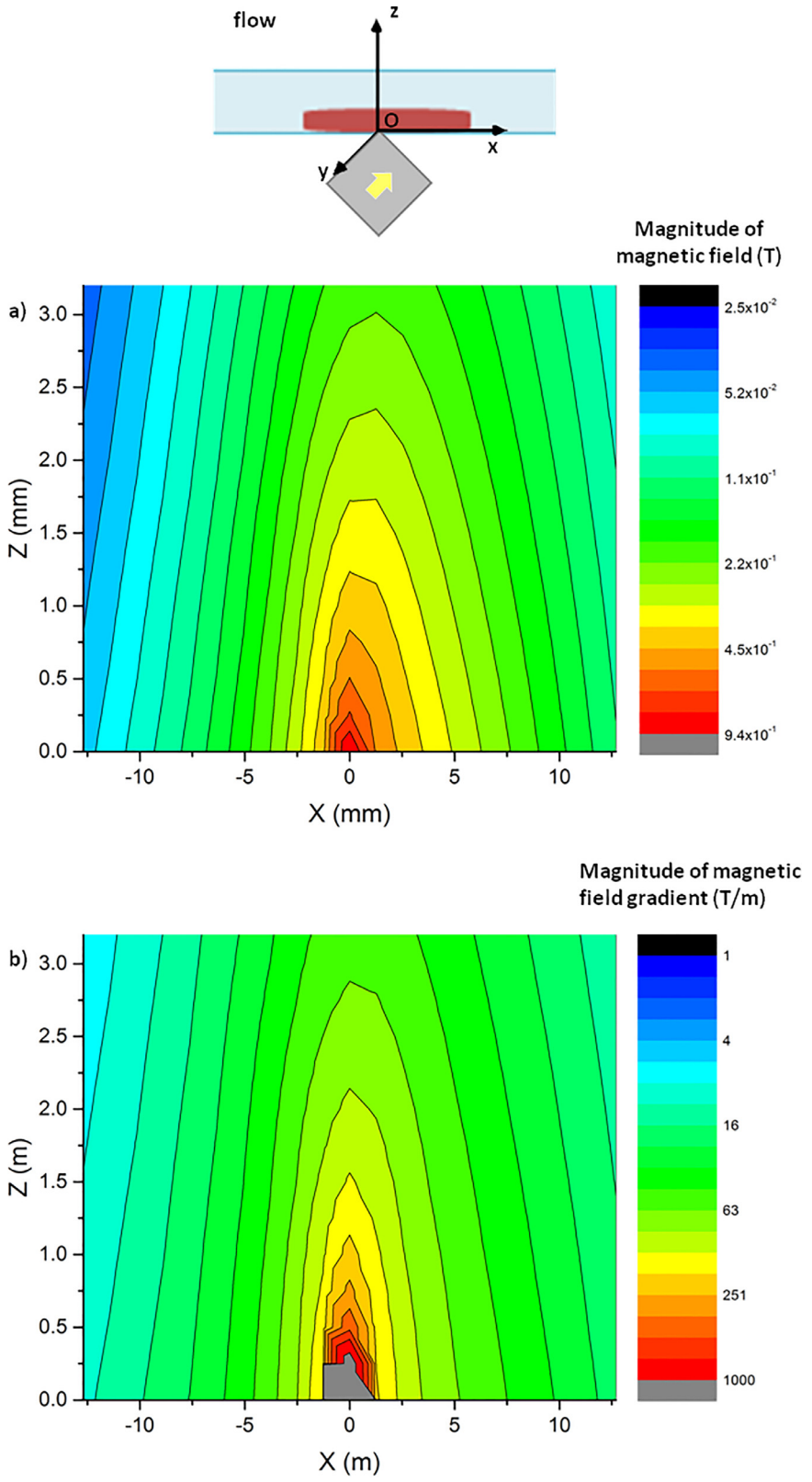

Fig. 2. Simulated contours of the magnetic field created by the magnet in the axial plane of the flow chamber. (a) Magnitude of magnetic field. (b) Magnitude of magnetic field gradient, $\nabla \mathbf{B}$. Inset (top): Origin, orientation of the axes and magnetisation vector (*yellow arrow*). The y-axis points into the page.

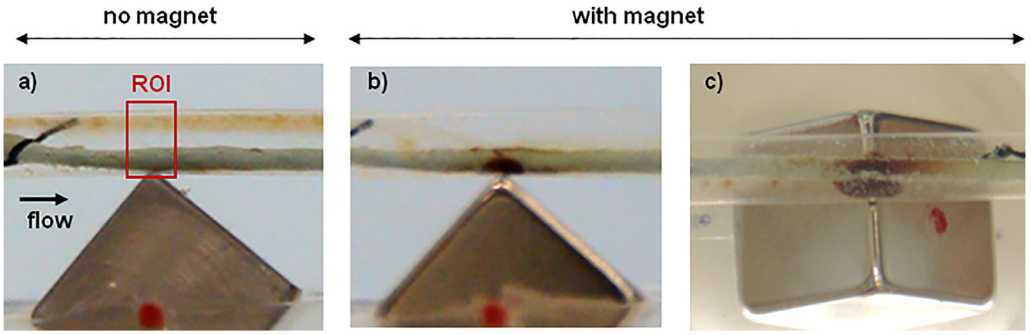

Fig. 3. Magnetic microbubble retention in the experimental setup. Magnetic microbubbles (brown suspension at the top of the channel) flow past a model clot (light-coloured cylinder at the bottom of the channel) in the absence and in the presence of a magnet. (a) Front view, control. ROI is the region of interest for image analysis. (b) Front view enlarged, with magnet. (c) Top view, with magnet. For reference, the length of each side of the magnet was 12.7 mm.

the left-hand section is the lysed region. The right-hand section was not in the US focal region.

Effect of magnetic targeting on acoustic emissions

The acoustic emissions from the US focal region were monitored throughout treatment. As evidenced by the illustrative frequency-domain traces of acoustic emissions in Figure 7, the acoustic emissions observed under excitation conditions of 0.5 MHz and a peak rarefactional pressure of 630 kPa are primarily broadband in nature, which is consistent with previous investigations (Arvanitis et al. 2011). No effort was therefore made to separate broadband from narrowband emissions, and the total energy of acoustic emissions can be taken as indicative of inertial cavitation.

Figure 7 also provides the mean and standard deviation of the total energy emitted in the frequency range was 2−5 MHz for each experimental group.

The use of microbubbles was associated with a significant increase in acoustic emissions over the US + tPA group ($p < 0.01$). In addition, there was a significant increase in acoustic emissions with US + tPA + microbubbles + magnet over US + tPA + microbubbles ($p < 0.01$). This validates the hypothesis that magnetic targeting enhances cavitation energy in the focal region by increasing the concentration of cavitation nuclei.

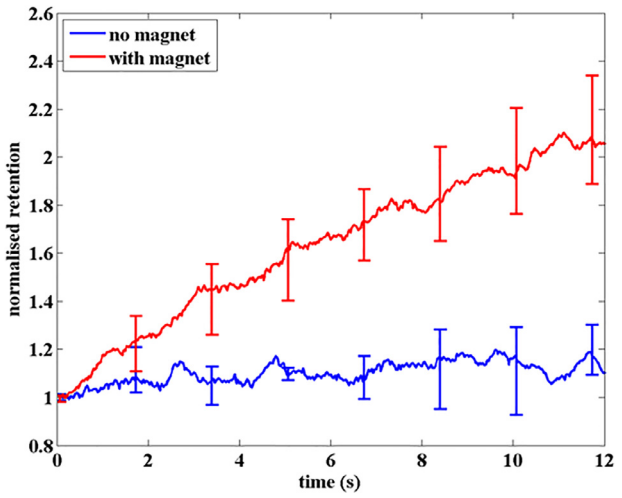

Fig. 4. Accumulation of magnetic material in the focal region of the 0.5-MHz transducer over 12 s with (red line) and without (blue line) magnetic targeting (n = 3). A 1-mL bolus of the microbubble stock solution was injected into the flow, and images were acquired at 30 frames/s according to the procedure described under Methods. Normalised retention at a given time point t is defined as the total gray-scale intensity in the region of interest at this time point, divided by the total gray-scale intensity at t = 0. Error bars represent the ranges of values observed.

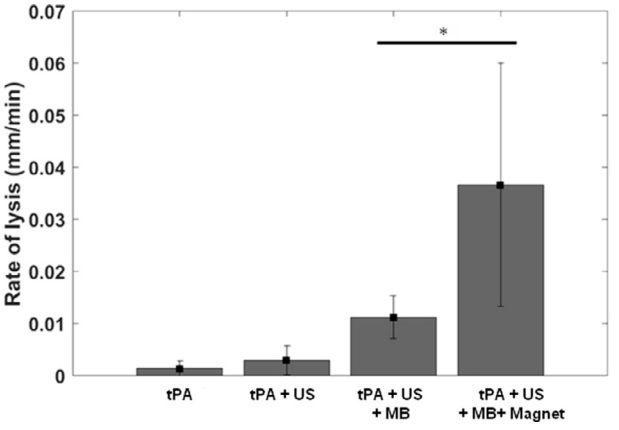

Fig. 5. Lysis rates during enzymatic sonothrombolysis of retracted porcine clots with magnetically targeted microbubbles (n = 6). The clots were treated with tPA (0.75 μg/mL) and 0.5-MHz US (630-kPa peak rarefactional pressure, 0.2-Hz pulse repetition frequency and 2% duty cycle). The maximum depth of clot lysis was computed from photographs taken every 30 s during treatment, yielding the lysis rate. Error bars represent standard deviations from the mean. Significance (*$p < 0.05$) was calculated with an analysis of variance followed by the Tukey post hoc test. MB = microbubbles; tPA = tissue plasminogen activator; US = ultrasound.

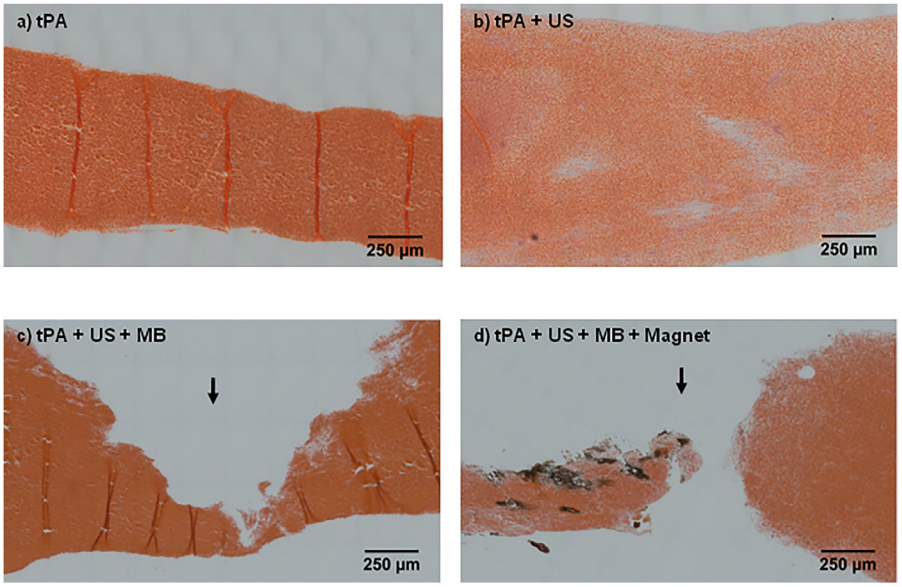

Fig. 6. Histologic samples of porcine clots after enzymatic thrombolysis. The clots were treated for 60 min with (a) tPA (0.75 μg/mL) only; (b) tPA and 0.5-MHz US (direction of propagation: *black arrows*; 630-kPa peak rarefactional pressure, 0.2-Hz pulse repetition frequency and 2% duty cycle); (c) tPA, US and magnetic microbubbles in the absence of a magnetic field; and (d) tPa, US and magnetic microbubbles in the presence of a magnetic field. The clots were fixed in formalin, embedded in paraffin and stained with eosin and hematoxylin. The striations seen in panels a and c are thought to have been produced during sectioning of the clot by the serrated edge of the blade used. MB = microbubbles; tPA = tissue plasminogen activator; US = ultrasound.

Investigating the potential of acoustic treatment monitoring

Acoustic emissions in the focal region were investigated as a potential indicator of treatment success. Lysis rates were plotted against acoustic emissions in the range 2−5 MHz (Fig. 8). There was found to be a positive correlation between acoustic emissions and lysis rates. Linear fitting yielded a coefficient of $R^2 = 0.870$ with $p < 0.01$. It was deemed that there were insufficient data to fit more complex curves.

Clot debris

The effluent was collected during treatment and analysed. In all experimental groups, more than 99.9% of the particles were smaller than 10 μm, that is, similar in size to red blood cells, indicating that the risk of downstream embolisation with this treatment is low.

DISCUSSION

In this study, magnetic targeting was associated with a significant increase in cavitation energy near the clot, confirming previous reports that magnetically targeted microbubbles can locally enhance cavitation (Crake et al. 2015). As this enhanced cavitation was associated with accelerated clot lysis, this study illustrates that magnetic targeting has the potential for a doubly positive impact on thrombolysis. Firstly, it may accelerate vessel recanalisation, increasing tissue salvage and limiting the adverse side effects associated with prolonged US exposure. These findings are particularly promising in the context of ischaemic stroke therapy, where early tissue reperfusion is crucial to improve patient outcomes (Rha and Saver 2007). Secondly, stronger cavitation signals may facilitate real-time treatment monitoring and thus enhance patient tolerability.

To the best of the authors' knowledge, this is the first report of magnetically targeted microbubbles as a method to accelerate sonothrombolysis. Targeted sonothrombolysis has been previously investigated *in vitro* and *in vivo* using various "biological" microbubble targeting methods (*e.g.,* antibody conjugation) (Alonso et al. 2009; Chen et al. 2009; Culp et al. 2004; Wu et al. 1998; Xie et al. 2009b). Higher plasma D-dimer levels have been reported in rats treated with pulsed 2-MHz US and platelet-specific, abciximab-coated immunobubbles, compared with the non-specific immunobubble control group. Histologic analysis also revealed clot disintegration in four of five clots in the targeted group, compared with one of five clots in the controls (Alonso et al. 2009; Xie et al. 2009b). investigated glycoprotein IIb/IIIa−targeted microbubbles in a porcine model of arterial thrombosis, in the presence of prourokinase. The authors reported that, compared with control microbubbles, the targeted bubbles were associated with significantly greater replenishment of contrast

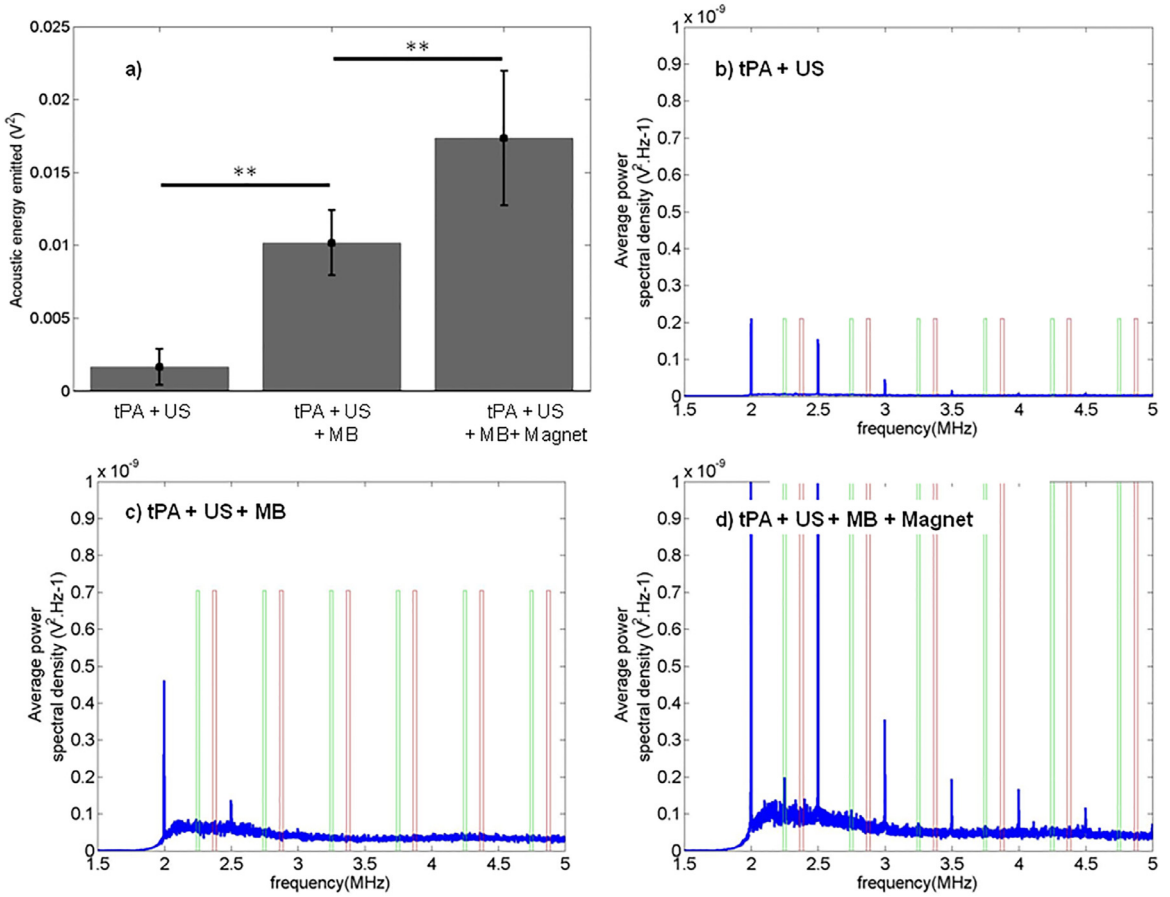

Fig. 7. Acoustic energy detected during sonothrombolysis of retracted porcine clots with magnetically targeted microbubbles (n = 6). The clots were treated with tPA (0.75 μg/mL) and 0.5-MHz US (630-kPa peak rarefactional pressure, 0.2-Hz pulse repetition frequency and 2% duty cycle). The acoustic emissions at the focus were acquired with a 7.5-MHz passive cavitation detector transducer mounted coaxially with the 0.5-MHz transducer. Error bars represent standard deviations from the mean. (a) Total energy in the frequency range 2−5 MHz. Significance (**$p < 0.01$) was calculated with a two-way analysis of variance followed by the Tukey *post hoc* test. (b) Illustrative frequency-domain trace of received acoustic emissions in the tPA + US group. (c) Illustrative frequency-domain trace of received acoustic emissions in the tPA + US + MB group. (d) Illustrative frequency-domain trace of received acoustic emissions in the t-PA + US + MB + magnet group. The *green and red rectangles* respectively frame 25-kHz-wide ultraharmonic and broadband regions, illustrating that the emissions are primarily broadband in nature. MB = microbubbles; tPA = tissue plasminogen activator; US = ultrasound.

agents in the at-risk area of the myocardium after 15 min of treatment. Alternative approaches to biologically targeted sonothrombolysis have also utilised other US-responsive particles. Tiukinhoy-Laing et al. (2007) developed fibrin-targeted, tPA-loaded echogenic liposomes. When exposed to 120-kHz US, these particles achieved more effective thrombolysis *in vitro* than free tPA + US. In comparison to these biologically targeted agents, the main advantage of magnetically targeted microbubbles is the relatively long potential working distance: magnetically targeted agents do not need to be initially in contact with the target to be retained. This property is particularly relevant in the context of thrombosed vessels, which are characterised by reduced blood flow and complex haemodynamic patterns (Strony et al. 1993; Wootton and Ku 1999).

Other researchers have provided an *in vitro* proof-of-concept for magnetically targeted enzymatic sonothrombolysis, developing magnetic polymer microparticles that release tPA upon exposure to very low frequency US (Kaminski et al. 2008; Torno et al. 2008). The present study uses magnetic microbubbles, which have the added advantage of strongly promoting cavitation. The microbubbles were effectively retained against physiologic flow rates using a magnetic field within the $8-3.8 \times 10^{-2}$ T range and a magnetic field gradient of 12−140 T/m. Such flux density and flux density gradients are achievable with permanent magnet arrays at

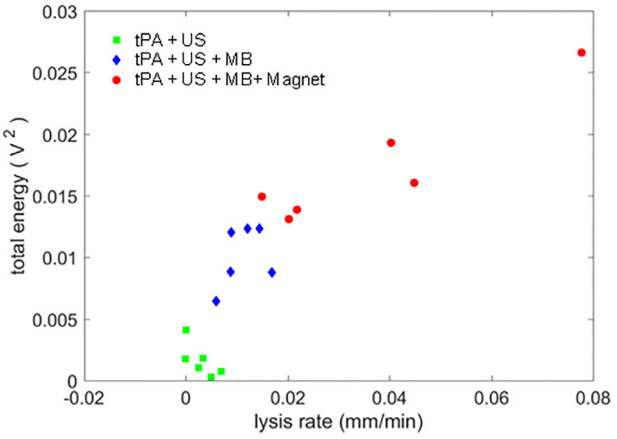

Fig. 8. Bivariate representation of lysis rate and total acoustic energy detected in the range 2−5 MHz. The clots were treated with tPA (0.75 μg/mL) and 0.5-MHz ultrasound (630-kPa peak rarefactional pressure, 0.2-Hz pulse repetition frequency and 2% duty cycle). Maximum depth of clot lysis was computed on photographs taken every 30 s during treatment, yielding the lysis rate. The acoustic emissions at the focus were acquired with a 7.5-MHz passive cavitation detector transducer mounted coaxially with the 0.5-MHz transducer.

depths up to a few tens of millimeters in the body depending on the flow rate (Barnsley et al. 2015, 2016; Owen et al. 2015). This is sufficient for treating clots in the middle cerebral artery (Gillard et al. 1986), one of the brain vessels most commonly affected by ischaemic stroke (Demchuk et al. 2001).

The results of this study suggest that sonothrombolysis can enable a reduction in the quantity of drug required. The drug alone did not produce significant lysis, which is attributable to the relatively short time frame of the experiment (60 min), the low concentration of tPA (0.75 μg/mL) compared with clinical doses and the use of porcine blood and plasma (Huang et al. 2017). Even under these conditions, substantial lysis acceleration occurred with US and non-targeted microbubbles. This is in agreement with previous studies that reported the possibility of lowering administered drug doses when using US and microbubbles (Brown et al. 2011; Petit et al. 2012). For instance, Brown et al. found *in vitro* that with pulsed 1-MHz US and albumin/dextrose microbubbles, tPA concentration could be reduced up to five times while maintaining thrombolytic efficacy. These results are encouraging in terms of patient tolerability, as lower doses of tPA could reduce the risk of intracranial haemorrhage in acute stroke management.

The results also indicate the feasibility of non-invasive treatment monitoring using passive cavitation detection, with good correlation between lysis rates and acoustic emissions. This contrasts with a previous study, in which whole porcine blood clots were exposed to tPA, pulsed US and lipid-shelled microbubbles (Datta et al. 2008). The authors reported a strong correlation between final clot lysis and ultraharmonic emissions ($R^2 = 0.83$, $p < 0.001$) and no correlation between lysis and broadband emissions. Under the acoustic conditions reported (120 kHz, 320 kPa, no flow), however, most of the emissions occurred in the harmonic and ultraharmonic ranges, whereas in the present study, the emissions occurred primarily in the broadband range. These findings suggest that the frequency range providing the most useful indicator of lytic success may depend upon the cavitation regime in the focal region and on the ratio between the wavelength and the mean bubble size. This is an area of active research (Bader et al. 2015; Petit et al. 2015; Porter et al. 2017) requiring further investigation.

The finding that sonothrombolysis can be significantly enhanced in an inertial cavitation regime warrants further discussion both in terms of potential mechanism and in terms of tolerability. Mechanistically, microstreaming has been routinely associated with non-inertial cavitation, primarily because of the need for persistent cavitation to occur for a stable microstreaming field to be established. However, several recent studies in the context of cancer drug delivery have indicated that suitably nucleated, sustained inertial cavitation in fact results in higher streaming velocities than non-inertial cavitation *in vitro* (Rifai et al. 2010) and enables significantly enhanced drug delivery, penetration and distribution *in vivo* (Arvanitis et al. 2011). These recent findings suggest that strategies that enable sustained inertial cavitation to occur, such as the magnetic retention approach described here, could offer significant enhancements in terms of drug transport and penetration.

In terms of tolerability, inertial cavitation has traditionally been deemed undesirable for diagnostic and therapeutic applications, in great part because of reports of a higher incidence of unwanted bio-effects (Schafer et al. 2005). Over the past decade, studies specifically aimed at opening the blood−brain barrier have further indicated that inertial cavitation can cause undesirable erythrocyte extravasation and cell death in murine brain models (McDannold et al. 2006). However, a recent clinical study on opening the blood−brain barrier in humans (Carpentier et al. 2016) reported no tolerability concerns at peak rarefactional pressure amplitudes up to 1.1 MPa at a frequency of 1.05 MHz, which would result in inertial cavitation in the presence of microbubbles. A key feature of this clinical study was that the US excitation was highly localized through a transcranially implanted probe, even though both the microbubbles and the drug were systemically administered. Similarly, it is conceivable that an approach that localizes and only locally enhances inertial cavitation could ultimately present a clinically acceptable safety profile.

Limitations

The study has a number of limitations that warrant comment. The model mimics a partial vessel occlusion, which does not perfectly represent most *in vivo* pathologic thrombi, although partial occlusions may also lead to acute clinical symptoms (Chesebro et al. 1987; Xie et al. 2009a). A single-vessel orientation (horizontal) was investigated in the present study; future work may focus on the effect of different orientation angles, to mimic a broader range of clinical and physiologic conditions. Also, blood from a single animal was used here. The range of hematocrits in the porcine blood used for the current work was consistently found to be in the range 25%−30%, and clots were assigned to individual groups blindly to mitigate the possibility of bias. Nevertheless, in future studies, samples from multiple animals may be pooled to limit the effects of pig-to-pig variability. To further increase clinical relevance, the composition of the plasma solution in the flow loop may also be improved. A recent study by Huang et al. (2017) reported that using human plasminogen in the liquid surrounding a porcine clot produces sonothrombolysis behaviours that more closely resemble human clots in human plasma.

In addition, many published studies use traveling waves when studying sonothrombolysis (Datta et al. 2006; Petit et al. 2012; Pfaffenberger et al. 2005; Xie et al. 2009b), whereas the US field in this study included a partial standing wave. This is inherent to the geometry of the setup. It is not expected to affect microbubble oscillations, as the size of a microbubble (∼1−10 μm) is much smaller than half the wavelength at 0.5 MHz (∼1.5 mm), but it may have affected microbubble translation. In clinical applications, standing waves are generally not desirable for patient tolerability (Baron et al. 2009; Daffertshofer et al. 2005), although standing waves may also form *in vivo* in transcranial applications (Baron et al. 2009; Bouchoux et al. 2014). Furthermore, the microbubble formulation used was not optimal for human use because of its composition. Magnetic microbubble formulations with improved biocompatibility have recently been developed and characterized, and will be used in future work (Owen et al. 2012). Finally, the physical properties of the flow medium did not faithfully replicate blood's properties, which may affect microbubble flow behaviour and acoustic response. Future studies will be conducted using whole blood, which may require changes to the optical imaging technique employed to quantify clot lysis (because of the reduced image quality).

CONCLUSIONS

This study illustrates *in vitro* that magnetic targeting can significantly accelerate microbubble-enhanced enzymatic sonothrombolysis at 0.5 MHz, with the potential to reduce administered drug doses and achieve faster vessel recanalisation. A greater than threefold increase in the lysis rate was observed when using magnetic targeting, compared with microbubbles in the absence of magnetic force. The total energy of acoustic emissions was strongly correlated with lytic rates, providing a possible method for real-time treatment monitoring. These results indicate that magnetic targeting has the potential to enhance treatment efficacy and patient tolerability in the management of occlusive conditions using microbubble-mediated sonothrombolysis.

Acknowledgments—The authors gratefully acknowledge the assistance of Paul Lyon and Murali Somasundaram in the blood collection process. They are also indebted to Jim Fisk and David Salisbury for their skilful fabrication of the flow setup and to Richard Stillion for his advice on the clot histopathology. The work was supported by funding from the Research Council UK Digital Economy Programme, through the Centre for Doctoral Training in Healthcare Innovation (Grant EP/G036861/1) and the Engineering and Physical Sciences Research Council (EPSRC Grant EP/I021795/1). Supporting data are available through the University of Oxford ORA data repository https://ora.ox.ac.uk

REFERENCES

Alkatheri A. Stability of recombinant tissue plasminogen activator at −30˚C over one year. Pharmaceuticals 2013;6:25–31.

Alonso A, Dempfle CE, Della Martina A, Stroick M, Fatar M, Zohsel K, Allemann E, Hennerici MG, Meairs S. In vivo clot lysis of human thrombus with intravenous abciximab immunobubbles and ultrasound. Thromb Res 2009;124:70–74.

American College of Emergency Physicians, American Academy of Neurology. Clinical policy: Use of intravenous tPA for the management of acute ischemic stroke in the emergency department. Ann Emerg Med 2013;61:225–243.

Arvanitis CD, Bazan-Peregrino M, Rifai B, Seymour LW, Coussios CC. Cavitation-enhanced extravasation for drug delivery. Ultrasound Med Biol 2011;37:1838–1852.

Bader KB, Gruber MJ, Holland CK. Shaken and stirred: Mechanisms of ultrasound-enhanced thrombolysis. Ultrasound Med Biol 2015;41:187–196.

Barber PA, Zhang J, Demchuk AM, Hill MD, Buchan AM. Why are stroke patients excluded from TPA therapy? An analysis of patient eligibility. Neurology 2001;56:1015–1020.

Barnsley LC, Carugo D, Owen J, Stride E. Halbach arrays consisting of cubic elements optimised for high field gradients in magnetic drug targeting applications. Phys Med Biol 2015;60:8303–8327.

Barnsley LC, Carugo D, Stride E. Optimized shapes of magnetic arrays for drug targeting applications. J Phys D Appl Phys 2016;49 225501.

Baron C, Aubry JF, Tanter M, Meairs S, Fink M. Simulation of intracranial acoustic fields in clinical trials of sonothrombolysis. Ultrasound Med Biol 2009;35:1148–1158.

Bouchoux G, Shivashankar R, Abruzzo TA, Holland CK. In silico study of low-frequency transcranial ultrasound fields in acute ischemic stroke patients. Ultrasound Med Biol 2014;40:1154–1166.

Brown AT, Flores R, Hamilton E, Roberson PK, Borrelli MJ, Culp WC. Microbubbles improve sonothrombolysis *in vitro* and decrease hemorrhage *in vivo* in a rabbit stroke model. Invest Radiol 2011;46:202–207.

California Acute Stroke Pilot Registry Investigators. Prioritizing interventions to improve rates of thrombolysis for ischemic stroke. Neurology 2005;64:654–659.

Carpentier A, Canney M, Vignot A, Reina V, Beccaria K, Horodyckid C, Karachi C, Leclercq D, Lafon C, Chapelon JY, Capelle L, Cornu P, Sanson M, Hoang-Xuan K, Delattre JY, Idbaih A. Clinical trial of

blood–brain barrier disruption by pulsed ultrasound. Sci Transl Med 2016;8:343re2.
Chen SC, Ruan JL, Cheng PW, Chuang YH, Liz PC. In vitro evaluation of ultrasound-assisted thrombolysis using a targeted ultrasound contrast agent. Ultrason Imaging 2009;31:235–246.
Chesebro JH, Knatterud G, Roberts R, Borer J, Cohen LS, Dalen J, Dodge HT, Francis CK, Hillis D, Ludbrook P, Markis JE, Mueller H, Passamani ER, Powers ER, Rao AK, Robertson T, Ross A, Ryan TJ, Sobel BE, Willerson J, Williams DO, Zaret BL, Braunwald E. Thrombolysis in myocardial infarction (TIMI) Trial, Phase I: A comparison between intravenous tissue plasminogen-activator and intravenous streptokinase. Clinical findings through hospital discharge. Circulation 1987;76:142–154.
Crake C, Saint Victor MD, Owen J, Coviello C, Collin J, Coussios CC, Stride E. Passive acoustic mapping of magnetic microbubbles for cavitation enhancement and localization. Phys Med Biol 2015;60:785–806.
Culp WC, Porter TR, Lowery J, Xie F, Roberson PK, Marky L. Intracranial clot lysis with intravenous microbubbles and transcranial ultrasound in swine. Stroke 2004;35:2407–2411.
Daffertshofer M, Gass A, Ringleb P, Sitzer M, Sliwka U, Els T, Sedlaczek O, Koroshetz WJ, Hennerici MG. Transcranial low-frequency ultrasound-mediated thrombolysis in brain ischemia: Increased risk of hemorrhage with combined ultrasound and tissue plasminogen activator: Results of a phase II clinical trial. Stroke 2005;36: 1441–1446.
Datta S, Coussios CC, McAdory LE, Tan J, Porter T, De Courten-Myers G, Holland CK. Correlation of cavitation with ultrasound enhancement of thrombolysis. Ultrasound Med Biol 2006;32: 1257–1267.
Datta S, Coussios CC, Ammi AY, Mast TD, de Courten-Myers GM, Holland CK. Ultrasound-enhanced thrombolysis using Definity® as a cavitation nucleation agent. Ultrasound in Med Biol 2008;34:1421–1433.
de Saint Victor M, Carugo D, Barnsley LC, Owen J, Coussios CC, Stride E. Magnetic targeting to enhance microbubble delivery in an occluded microarterial bifurcation. Phys Med Biol 2017;62: 7451–7470.
Demchuk AM, Burgin WS, Christou I, Felberg RA, Barber PA, Hill MD, Alexandrov AV. Thrombolysis in brain ischemia (TIBI) transcranial Doppler flow grades predict clinical severity, early recovery, and mortality in patients treated with intravenous tissue plasminogen activator. Stroke 2001;32:89–93.
Engel-Herbert R, Hesjedal T. Calculation of the magnetic stray field of a uniaxial magnetic domain. J Appl Phys 2005;97: 074504.
Feigin V, Norrving B, Mensah G. global burden of stroke. Circ Res 2017;120:439–448.
GBD 2013 Mortality and Causes of Death Collaborators. Global, regional, and national age-sex specific all-cause and cause-specific mortality for 240 causes of death, 1990–2013: A systematic analysis for the Global Burden of Disease Study 2013. Lancet 2015;385:117–171.
Gillard JH, Kirkham FJ, Levin SD, Neville BG, Gosling RG. Anatomical validation of middle cerebral artery position as identified by transcranial pulsed Doppler ultrasound. J Neurol Neurosurg Psychiatry 1986;49:1025–1029.
Hagisawa K, Nishioka T, Suzuki R, Maruyama K, Takase B, Ishihara M, Kurita A, Yoshimoto N, Nishida Y, Iida K, Luo H, Siegel RJ. Thrombus-targeted perfluorocarbon-containing liposomal bubbles for enhancement of ultrasonic thrombolysis: In vitro and in vivo study. J Thromb Haemost 2013;11:1565–1573.
Hockham N, Coussios CC, Arora M. A Real-time controller for sustaining thermally relevant acoustic cavitation during ultrasound therapy. IEEE Trans Ultrason Ferroelectr Freq Control 2010;57: 2685–2694.
Holland CK, Vaidya SS, Datta S, Coussios CC, Shaw GJ. Ultrasound-enhanced tissue plasminogen activator thrombolysis in an *in vitro* porcine clot model. Thromb Res 2008;121:663–673.
Hua X, Zhou L, Liu P, He Y, Tan K, Chen Q, Gao Y, Gao Y. In vivo thrombolysis with targeted microbubbles loading tissue plasminogen activator in a rabbit femoral artery thrombus model. J Thromb Thrombolysis 2014;38:57–64.
Huang S, Shekhar H, Holland CK. Comparative lytic efficacy of rt-PA and ultrasound in porcine versus human clots. PLoS One 2017;12 e0177786.
Jaffe GJ, Green GDJ, Abrams GW. Stability of recombinant tissue plasminogen activator. Am J Ophthalmol 1989;108:90–91.
Kaminski MD, Xie YM, Mertz CJ, Finck MR, Chen HT, Rosengart AJ. Encapsulation and release of plasminogen activator from biodegradable magnetic microcarriers. Eur J Pharm Sci 2008;35:96–103.
Lu Y, Wang J, Huang R, Chen G, Zhong L, Shen S, Zhang C, Li X, Cao S, Liao W, Liao Y, Bin J. Microbubble-mediated sonothrombolysis improves outcome after thrombotic microembolism-induced acute ischemic stroke. Stroke 2016;47:1344–1353.
McDannold N, Vykhodtseva N, Hynynen K. Targeted disruption of the blood–brain barrier with focused ultrasound: Association with cavitation activity. Phys Med Biol 2006;51:793–807.
Meunier JM, Holland CK, Lindsell CJ, Shaw GJ. Duty cycle dependence of ultrasound enhanced thrombolysis in a human clot model. Ultrasound Med Biol 2007;33:576–583.
Molina CA, Ribo M, Rubiera M, Montaner J, Santamarina E, Delgado-Mederos R, Arenillas JF, Huertas R, Purroy F, Delgado P, Alvarez-Sabin J. Microbubble administration accelerates clot lysis during continuous 2-MHz ultrasound monitoring in stroke patients treated with intravenous tissue plasminogen activator. Stroke 2006;37:425–429.
Nedelmann M, Brandt C, Schneider F, Eicke BM, Kempski O, Krummenauer F, Dieterich M. Ultrasound-induced blood clot dissolution without a thrombolytic drug is more effective with lower frequencies. Cerebrovasc Dis 2005;20:18–22.
Nedelmann M, Reuter P, Walberer M, Sommer C, Alessandri B, Schiel D, Ritschel N, Kempski O, Kaps M, Mueller C, Bachmann G, Gerriets T. Detrimental effects of 60 kHz sonothrombolysis in rats with middle cerebral artery occlusion. Ultrasound Med Biol 2008;34:2019–2027.
National Institute for Health and Care Excellence (NICE). Stroke and transient ischaemic attack in over 16s: Diagnosis and initial management. Clinical guideline CG68. London: Author; 2008.
Ogata T, Kimura K, Nakajima M, Ikeno K, Naritomi H, Minematsu K. Transcranial color-coded real-time sonographic criteria for occlusion of the middle cerebral artery in acute ischemic stroke. AJNR Am J Neuroradiol 2004;25:1680–1684.
Owen J, Zhou B, Rademeyer P, Tang MX, Pankhurst Q, Eckersley R, Stride E. Understanding the structure and mechanism of formation of a new magnetic microbubble formulation. Theranostics 2012;2:1127–1139.
Owen J, Rademeyer P, Chung D, Cheng Q, Holroyd D, Coussios C, Friend P, Pankhurst QA, Stride E. Magnetic targeting of microbubbles against physiologically relevant flow conditions. Interface Focus 2015;5 20150001.
Perren F, Loulidi J, Poglia D, Landis T, Sztajzel R. Microbubble potentiated transcranial duplex ultrasound enhances IV thrombolysis in acute stroke. J Thromb Thrombolysis 2008;25:219–223.
Petit B, Gaud E, Colevret D, Arditi M, Yan F, Tranquart F, Allemann E. In vitro sonothrombolysis of human blood clots with BR38 microbubbles. Ultrasound Med Biol 2012;38:1222–1233.
Petit B, Bohren Y, Gaud E, Bussat P, Arditi M, Yan F, Tranquart F, Allemann E. Sonothrombolysis: The contribution of stable and inertial cavitation to clot lysis. Ultrasound Med Biol 2015;41: 1402–1410.
Pfaffenberger S, Devcic-Kuhar B, Kollmann C, Kastl SP, Kaun C, Speidl WS, Weiss TW, Demyanets S, Ullrich R, Sochor H, Wober C, Zeitlhofer J, Huber K, Groschl M, Benes E, Maurer G, Wojta J, Gottsauner-Wolf M. Can a commercial diagnostic ultrasound device accelerate thrombolysis? An *in vitro* skull model. Stroke 2005;36:124–128.
Porter TR, Xie F, Lof J, Powers J, Vignon F, Shi W, White M. The thrombolytic effect of diagnostic ultrasound-induced microbubble cavitation in acute carotid thromboembolism. Invest Radiol 2017;52:477–481.
Rha JH, Saver JL. The impact of recanalization on ischemic stroke outcome: A meta-analysis. Stroke 2007;38:967–973.

Rifai B, Arvanitis CD, Bazan-Peregrino M, Coussios CC. Cavitation-enhanced delivery of macromolecules into an obstructed vessel. J Acoust Soc Am 2010;128:EL310–EL315.

Schafer S, Kliner S, Klinghammer L, Kaarmann H, Lucic I, Nixdorff U, Rosenschein U, Daniel WG, Flachskampf FA. Influence of ultrasound operating parameters on ultrasound-induced thrombolysis *in vitro*. Ultrasound Med Biol 2005;31:841–847.

Schleicher N, Tomkins AJ, Kampschulte M, Hyvelin JM, Botteron C, Juenemann M, Yeniguen M, Krombach GA, Kaps M, Spratt NJ, Gerriets T, Nedelmann M. Sonothrombolysis with BR38 microbubbles improves microvascular patency in a rat model of stroke. PLoS One 2016;11: e0152898.

Sennoga CA, Mahue V, Loughran J, Casey J, Seddon JM, Tang M, Eckersley RJ. On sizing and counting of microbubbles using optical microscopy. Ultrasound Med Biol 2010;36:2093–2096.

Serrador JM, Picot PA, Rutt BK, Shoemaker JK, Bondar RL. MRI measures of middle cerebral artery diameter in conscious humans during simulated orthostasis. Stroke 2000;31:1672–1678.

Stride E, Porter C, Prieto AG, Pankhurst Q. Enhancement of microbubble mediated gene delivery by simultaneous exposure to ultrasonic and magnetic fields. Ultrasound Med Biol 2009;35:861–868.

Strony J, Beaudoin A, Brands D, Adelman B. Analysis of shear-stress and hemodynamic factors in a model of coronary-artery stenosis and thrombosis. Am J Physiol 1993;265:H1787–H1796.

Tiukinhoy-Laing SD, Buchanan K, Parikh D, Huang SL, MacDonald RC, McPherson DD, Klegerman ME. Fibrin targeting of tissue plasminogen activator-loaded echogenic liposomes. J Drug Target 2007;15:109–114.

Torno MD, Kaminski MD, Xie YM, Meyers RE, Mertz CJ, Liu X, O'Brien WD, Rosengart AJ. Improvement of *in vitro* thrombolysis employing magnetically-guided microspheres. Thromb Res 2008;121:799–811.

U.S. Food and Drug Administration (FDA). Alteplase Product Approval Information. US Food and Drug Aministration Licensing Action, June 18, 1996;.

Wootton DgM, Ku DN. Fluid mechanics of vascular systems, diseases, and thrombosis. Annu Rev Biomed Eng 1999;1:299–329.

Wu YQ, Unger EC, McCreery TP, Sweitzer RH, Shen DK, Wu GL, Vielhauer MD. Binding and lysing of blood clots using MRX-408. Invest Radiol 1998;33:880–885.

Xie F, Lof J, Everbach C, He AM, Bennett RM, Matsunaga T, Johanning J, Porter TR. Treatment of acute intravascular thrombi with diagnostic ultrasound and intravenous microbubbles. JACC Cardiovasc Imaging 2009a;2:511–518.

Xie F, Lof J, Matsunaga T, Zutshi R, Porter TR. Diagnostic ultrasound combined with glycoprotein IIb/IIIa-targeted microbubbles improves microvascular recovery after acute coronary thrombotic occlusions. Circulation 2009b;119:1378–1385.